Science of the Total Environment 807 (2022) 151013

Contents lists available at ScienceDirect

Science of the Total Environment

journal homepage: www.elsevier.com/locate/scitotenv

An observational study of hydrodynamic impact on water mass transport due to tidal power generation

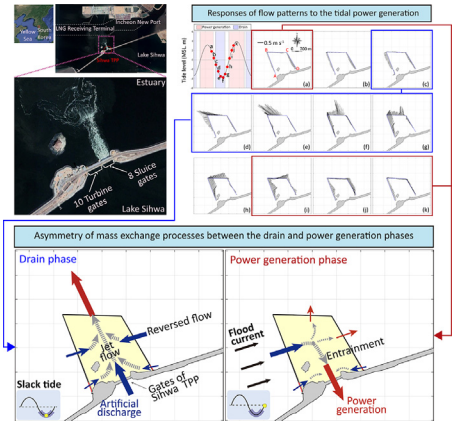
J.W. Kim [a], S.-B. Woo [a,*], J.I. Song [a], H.-K. Kwon [b]

[a] Department of Ocean Sciences, Inha University, Incheon 22212, Republic of Korea
[b] Korea Water Resources Corporation, Ansan 15637, Republic of Korea

HIGHLIGHTS

- Current speed during drain was 3 times stronger than that during power generation.
- Due to the jet-flow, the horizontal shear is high while the vertical shear is low.
- Mass transport patterns between power generation and drain phases were asymmetry.

GRAPHICAL ABSTRACT



ARTICLE INFO

Article history:
Received 15 July 2021
Received in revised form 8 October 2021
Accepted 11 October 2021
Available online 15 October 2021

Editor: Huu Hao Ngo

Keywords:
Renewable energy
Power generation
Jet-flow
Volume transport
Asymmetric water exchange

ABSTRACT

The world's largest Sihwa Tidal Power Plant (TPP), located on the west coast of Korea, was built in 2011 for the purpose of improving water quality and producing renewable energy. After several years of actual operation, most of the original purpose was achieved, but unexpected coastal environmental changes such as tidal flat damage and sediment accumulation also occurred. In this study, in order to understand the causes of these environmental changes, field observations were conducted near TPP, and spatial and temporal variability of flow structure and water exchange process were investigated. Three-dimensional velocity data were collected along the closed line surrounding the outside of the TPP for 11 h during spring tide and analyzed according to two discharge phases: power generation phase (PGP) and drainage phase (DP). The results show that the depth-averaged maximum current velocity was more than three times greater at DP than at PGP. Jet-like flow during DP caused very high horizontal shear, whereas vertical shear was relatively weak, indicating that the horizontal and vertical flow structures were very different. The most notable result is that the mass transport patterns between PGP and DP are significantly different, i.e., during PGP, mass transport is dominated on the left side of the TPP, whereas during DP, it occurs at the front of the TPP. This means that there is a strong spatiotemporal asymmetry between the inflow from the downstream (outside of the TPP) during PGP and the outflow from the upstream (inside of the TPP) during DP. These asymmetric processes can have a significant impact on the material exchange and sediment transport near the TPP. Since observational studies on TPP are extremely rare, this study is expected to contribute to future TPP related research, such as numerical modeling.

© 2021 Elsevier B.V. All rights reserved.

* Corresponding author at: Department of Ocean Sciences, Inha University, Incheon 22212, Republic of Korea.
E-mail addresses: sbwoo@inha.ac.kr, sbwoo@mpl.inha.ac.kr (S.-B. Woo).

https://doi.org/10.1016/j.scitotenv.2021.151013
0048-9697/© 2021 Elsevier B.V. All rights reserved.

1. Introduction

Tidal power generation is one of the most representative renewable energy resources (Charlier, 2003; Widén et al., 2015). Numerous tidal power plants (TPPs) have been operated or planned around the world (O'Rourke et al., 2010), each providing different economic benefits. However, TPPs typically require large-scale power generation facilities, which would inevitably lead to environmental changes in nearby regions (Wu et al., 2017). For instance, in the Rance estuary, the distribution of bed sediment changed from sand to mud after the operation of the La Rance TPP (Kirby and Retière, 2009). In the Severn Barrage system, numerical modeling was used to predict that the suspended sediment concentration (SSC) may significantly decrease after barrage construction (Ahmadian et al., 2014). In a numerical model study of the eastern Irish Sea, tidal deformations occurred in both the far-field and adjacent regions, leading to a decrease in intertidal zones (Wolf et al., 2009) and an increase of inundation problem due to sea-level rise (Nazarnia et al., 2020). Kadiri et al. (2012) also suggested that changes in the sedimentary environment resulting from the operation of TPPs could potentially affect dissolved nutrients and metal concentrations and impact the water quality and ecological functioning of marine systems. In the Sihwa TPP, the research area of this study, also has undergone various coastal environmental changes such as tidal flat damages and sediment accumulation in major sea routes.

One of the major causes affecting these environmental changes is the periodic discharge from the TPP (Xia et al., 2010; Cham et al., 2020). TPP discharges can cause increased flow intensity, vertical and horizontal mixing, and dispersal of materials into the surrounding waters. Yamini et al. (2021) suggested that the environmental impact range caused by dam discharge can be very considerable in reservoirs depending on the type of power generation method and the sluice structure. Angeloudis et al. (2016) indicated that accurate momentum calculation around TPP is very important for reliable environmental impact assessment due to the TPP construction in the Severn lagoon system. Kim et al. (2017) suggested that a strong flow and the resulting anticlockwise rotating vortex, showing great variability in response to the discharge, are key controlling factors in eroding the bed sediment and maintaining it in suspension. Rtimi et al. (2021) performed a detailed study of the discharge coefficient in a numerical model for the study of tidal asymmetry due to the Lance TPP construction. Artificial and periodic discharge from TPP can be considered as one of the main causes of environmental change because it inevitably affects the flow structure in the downstream area (outside of the TPP), which was a natural tidal environment before the TPP construction.

Since the previous studies were mainly conducted using numerical models and point measurement data, it was difficult to understand the spatial flow pattern during discharge, and there was a limitation in analyzing the mass transport process near the TPP in detail. In addition, most of the validation data used in the recent numerical modeling studies were observed far away from the TPP, so the effect of discharge cannot be directly analyzed from the observation data. Until recently, most studies related to tidal power generation utilize the numerical modeling, and there are few analytical studies based on field observation data during actual power plant operation.

In this study, three-dimensional velocity data over a tidal cycle were measured along a closed line where the actual discharge was directly affected at Sihwa TPP. By analyzing the observed data, we tried to understand the spatiotemporal flow structure near the TPP and the water mass exchange process. The purpose of this study is to: 1) investigate how the flow characteristics around the TPP occur during the operation, 2) compare the spatiotemporal mass transport patterns between power generation and drainage, 3) analyze the water exchange process between upstream (inside of TPP) and downstream through volume flux analysis. Based on this analysis, we would like to discuss the causes of changes in the tidal flat environment and sediment accumulation problems occurring near the Sihwa TPP. In addition, the results of this study are expected to be used not only for verification of numerical model studies related to TPP, but also for problems that require huge costs, such as periodic dredging of major routes.

The rest of the paper is organized as follows. In the next section, the study area was introduced, and the operation method of the Sihwa TPP was described. Section 3 summarizes the methods for collecting, processing, and analyzing observational data. Section 4 presents the spatiotemporal velocity structure during the power generation and drainage period and analyzes the volumetric transport. In Section 5, the water exchange process between upstream and downstream was analyzed and the effect on the surrounding area was discussed. Conclusions are summarized in Section 6.

2. Study area

The Sihwa area, located in the southern part of Gyeonggi Bay on the west coast of the Korean Peninsula, is well known as a suitable region for tidal power generation with the hyper-tidal estuary (Fig. 1a) (Kim et al., 2012; Park, 2017). The major tidal constituents are M_2, S_2, K_1, and O_1. The water level exhibits typical semi-diurnal tides with spring-neap variations. The mean spring and neap tidal ranges are 7.7 m and 3.3 m, respectively. The mean water depth is about 13 m. The Sihwa area was divided into Lake Sihwa (upstream) and the Sihwa estuary (downstream) after the construction of the Sihwa tide embankment in 1994. A small island with a diameter of 200 m is located 0.5 km away from the northwest of the TPP.

The tidal current before the construction of the TPP (background tidal current) was typically propagated from the southwest part of Daebudo, and its main flow direction was northeastward and southwestward during the flood and ebb currents, respectively (Fig. 1b) (Bae et al., 2017). After the operation of the Sihwa TPP began, the background tidal current patterns periodically turned northwestward (discharge direction), and a current speed of 2 m s^{-1} or more was observed near the TPP (Kim et al., 2017).

The Sihwa TPP consists of 10 hydraulic turbine gates and 8 sluice gates (Fig. 1c), and the parts of the turbine gate are equipped with bulb-type turbo generators. The power output of Sihwa TPP was represented by a function of the water head difference in the Hill Chart provided by the manufacturer (Kim et al., 2021). The operation of the Sihwa TPP, using a flood generation scheme, can be largely divided into upstream and downstream discharge phases: the power generation phase (PGP) and drain phase (DP) (Fig. 1d and e). The PGP is carried out only when the water level of Lake Sihwa is below −1 m relative to the mean-sea level (MSL). During this phase, for about 5–7 h, the seawater enters from upstream through the 10 hydraulic turbine gates. In contrast, DP is mostly carried out during the ebb current. In this phase, all 10 hydraulic turbines and the additional 8 sluice gates are used to export the seawater upstream into the downstream for about 1–2 h. The seawater exchanges of PGP and DP are carried out twice a day, with a maximum exchange volume of 150 million tons for each phase.

The Sihwa region in South Korea was no exception to marine environmental changes due to tidal power generation. Since the beginning of the Sihwa TPP operation in 2011, the environmental issues associated with the operation of the TPP have been as follows:

- A strong flow (>1.5 m s^{-1}) is periodically observed downstream, and this flow has an influence on the speed and direction of flow. Since there are sea routes and berth facilities for large vessels at Incheon New Port, this strong flow has a major risk factor for the safe operation of ships.
- The downstream water circulation patterns are disturbed by the operation of the Sihwa TPP, and as a result, the residence time of suspended sediment adjacent to Sorae Port (regions located in the northeastern part of the Sihwa TPP in Fig. 1a) have increased (Bae et al., 2017). Kim et al. (2017) suggested that a strong flow and the resulting anticlockwise rotating vortex, showing great variability in

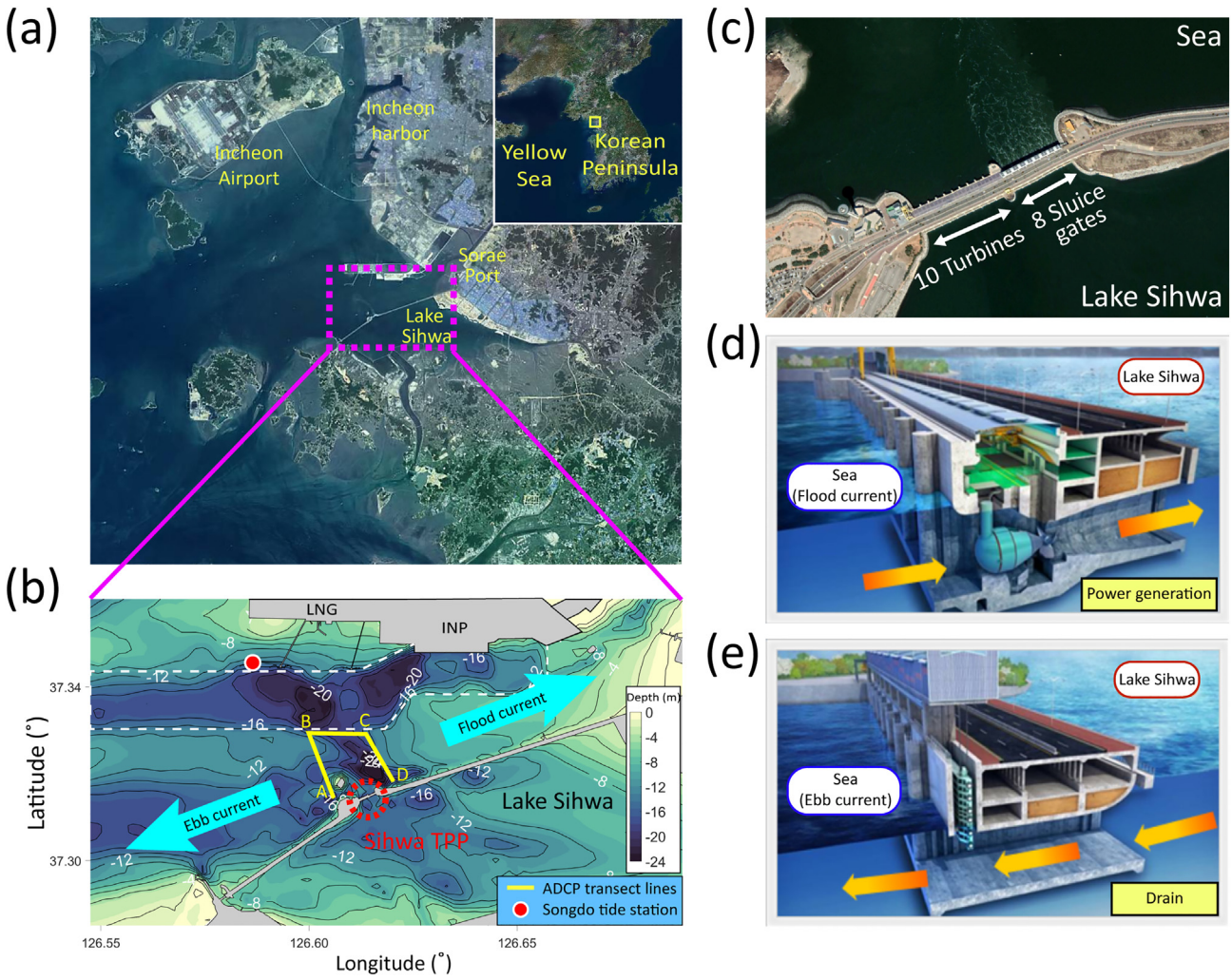


Fig. 1. (a) The location of the study area, the Sihwa tidal power plant (TPP), on the west coast of the Korean Peninsula, (b) plan view of the study area showing the bathymetric contours and sampling locations including the ADCP transect lines (yellow lines along ABCD with a total distance of about 3.89 km) and the Songdo tide station (red circle), (c) Satellite image near the Sihwa TPP (source: Google Earth), and schematic diagram for explaining water exchange during (d) power generation (PGP) and (e) drain phases (DP) of the Sihwa TPP (http://tlight.kwater.or.kr). In (b), INP denotes the Incheon New Port and the sky blue arrows indicate flood and ebb current directions.

response to the discharge, are key controlling factors in eroding the bed sediment and maintaining it in suspension.

- Tidal variations in water level, salinity, and temperature have been observed again in Lake Sihwa since the establishment of TPP (Kang et al., 2013). In contrast, heavy metals and pollutants stagnated in Lake Sihwa were reduced by an increase in seawater exchange (Susaya et al., 2011; Lee et al., 2014). Kim and Koo (2015) reported that the intertidal area increased from 5.6 km^2 in 2010 to 20 km^2 in 2013, and Kim et al. (2021) suggested that sediment accumulation in Lake Sihwa can occur because of unbalanced sediment transport associated with tidal power generation.

3. Materials and methods

The flow patterns near the Sihwa TPP change significantly in response to the operation time and exchanged water volume between the PGP and DP. To analyze this sensitively changing flow velocity distribution, the observation lines were set as a closed ABCD around the downstream. The notation used in this study is presented in Table 1. Surveys with the ship-mounted acoustic Doppler current profiler (ADCP, RDI 600 kHz) were conducted at transects AB, BC, and CD during the spring tide on February 5, 2015 (Fig. 2 and Table 2). The total distance of the three lines was about 3.89 km, and line locations were within a 1.5 km radius of the Sihwa TPP. The mean depth for each line was 13.8, 18.0, and 14.0 m, respectively. The velocity profile data along ABCD were collected 11 times over 9 h. The ADCP was installed 0.8 m below the surface, and the blanking distance was set to 1 m. The bin size was 0.5 m, and the data were obtained with two pings per second. The ship speeds varied between 1.5 and 2.5 m s^{-1}, and real-time latitude and longitude data were obtained by connecting a differential global positioning system (GPS) to a laptop. The downstream water level was obtained from the Songdo tide station (red circle in Fig. 1b).

A quality check and data processing for ADCP ensemble data were conducted to distinguish reliable records (Fig. 3). Data with sea surface exposure of ADCP and without GPS signals were discarded. Additionally, data with a Percent Good variable of less than 90, which showed the bad signal return rate, were omitted. The data with the pitch, roll, and head of ADCP tilted more than 8° were discarded. The data processing for velocity profiles described in Valle-Levinson and Atkinson (1999) was carried out. After removing outliers exceeding 2.5 standard deviations in velocity profile, the linear interpolation was performed on the empty data using the nearest neighbor data. In addition, the three-point average method proposed by Dinehart and Burau (2005) was applied to avoid the distorting velocity profiles. The compass and

Table 1
List of notations.

Symbol	Description
ABCD	total observation line along transects AB, BC, and CD
A′A	unmeasured line between the southern end of AB and the Sihwa tide embankment
DD′	unmeasured line between the southern end of CD and the Sihwa tide embankment
x, y, z	east, north, and vertical axes of Cartesian coordinate
u, v, w	velocity components in Cartesian coordinate
$\overline{u}$	depth-averaged velocity
U	normal velocity components on transects AB, BC, CD
D	time-varying total water depth
d	water depth of each ADCP bin
σ	normalized vertical axes by dividing the bin depth over the total water depth (d/D)
$u_\sigma, v_\sigma, w_\sigma$	velocity components in σ-coordinates
i	ensemble position
l	total number of ensembles
dx_i	distance between each ensemble
Q	instantaneous volume fluxes through transects AB, BC, and CD
$Q_{A'A}$	instantaneous volume fluxes through transect A′A
$Q_{DD'}$	instantaneous volume fluxes through transect DD′
L	distance between the Sihwa tide embankment and the last ADCP-measured position
V_m	measured cross-sectional averaged velocity at the nearest position to the unmeasured lines (A′A and DD′)
d_m	measured total water depth at the nearest position to the unmeasured lines (A′A and DD′)

magnitude errors of velocities derived from the ship velocity were corrected following Joyce (1989). The total observation lines were divided at equal intervals of 20 m, and the velocity profiles within the range were averaged to reduce the spatial data fluctuations.

The velocity data in the uppermost 1.8 m of the water column were not measured because of the deployment depth and blanking distance of the ADCP. In addition, the data observed within 1 m above the bottom were discarded due to the error velocity associated with the side-lobe effects. Therefore, the missing velocity profile data occupied at least 10% of the total depth, leading to an underestimation of the volume flux through transects. In this study, the velocity measured in the uppermost bin was used to fill the surface gap. The near-bed missing data were computed by curve fitting the one-sixth power law using the average of the last two measured velocities in the undermost bin with no slip at the bed (Mueller and Wagner, 2007).

The σ-coordinate system, which was normalized by dividing the observed depth over the total water depth, was used to estimate the volume fluxes along the ABCD. The velocity components in Cartesian coordinate (u and v) were transformed to velocity components in σ-coordinate (u_σ and v_σ) with 21 equally spaced σ-levels, where $\sigma = d/D$; d is the depth of each ADCP bin, and D is the time-varying total depth. Further, $\sigma = 0$ and $\sigma = 1$ are $d = 0$ (surface) and $d = D$ (seabed), respectively. This coordinate transformation is a suitable method for calculating the volume flux in a macrotidal estuary system (Giddings et al., 2014). The instantaneous volume flux (Q) was calculated as follows:

$$Q = D_i \sum_{i=1}^{l} U_{\sigma,i} dx_i, \tag{1}$$

where $U_{\sigma,i}$ represents the normal components of $u_{\sigma,i}$ and $v_{\sigma,i}$ on transects AB, BC, and CD (i represents ensemble positions), dx_i is the distance between each velocity ensemble, and l is the total number of velocity ensembles. The positive and negative Q correspond to the northwest- and southeast-ward volume fluxes, respectively, for transects AB and CD, and north- and south-ward volume fluxes, respectively, for transect BC.

The data for the total exchanged water volume through the sluice gate and operation time were obtained from the Korea Water Resources Corporation (http://tlight.kwater.or.kr) (Table 3). The gates for the seawater exchange were divided into three types of 8 turbine gates (G1), 8 sluice gates (G2), and one sluice gate at the entrance of Lake Sihwa (G3). The PGPs were conducted during the period of 02:38–08:11 and 14:43–21:05 on February 5, 2015, which introduced 8.75×10^7 m^3 and 10.74×10^7 m^3 of water into the lake, respectively. The DPs were conducted during the period of 00:00–01:00, 09:04–13:04, and 21:50–24:00, which discharged 1.54×10^7 m^3, 10.99×10^7 m^3, and 6.53×10^7 m^3 of water from the lake, respectively. The difference in total volume exchanged during PGP and DP was about 0.43×10^7 m^3, which was 0.01% of the Lake Sihwa volume of 32.38×10^7 m^3, as suggested by Bae et al. (2010).

4. Results

4.1. Velocity fields

To represent the spatial flow patterns along ABCD over an operation cycle of the Sihwa TPP, the stick plots of depth-averaged velocity ($\overline{u}$) are shown in Fig. 4. During the DP (Fig. 4c–g), the background tidal currents were greatly disturbed by the operation of the TPP. The direction and intensity of $\overline{u}$ at early in the DP (Fig. 4c) were not significantly different from those 1 h previously (Fig. 4b), and no influence on $\overline{u}$ associated with the discharge from a TPP was observed. As the DP progressed (Fig. 4d–g), the flow greater than 1 m s^{-1} associated with the discharge of TPP in transect BC was oriented nearly perpendicular to the ambient tidal current, with the peak $\overline{u}$ moving toward the eastern part of transect BC. During these periods in transect AB, the $\overline{u}$ turned from southwestward to northeastward. In contrast, a weak $\overline{u}$ (<0.2 m s^{-1}) toward the southwest was maintained in transect CD.

The complex flow patterns were observed at early in the PGP because the discharge effects of the DP remained (Fig. 4i). The $\overline{u}$ toward the northeast was observed in the central part of the AB and in the eastern part of BC, whereas that toward the southeast was observed in the northern end of AB and in the western part of BC. The $\overline{u}$ in transect CD was relatively weaker than that in transects AB and BC and complex patterns in $\overline{u}$ were exhibited with a local reversed flow pattern. As the PGP progressed, the flow in ABCD was rotated toward the Sihwa tide embankment. After 1–2 h of the start of the PGP (Fig. 4j and k), the $\overline{u}$ toward the northeast was observed in transect AB. During these periods in transects BC and CD, the $\overline{u}$ toward the southeast was dominant, but the $\overline{u}$ toward the southwest was observed at the southern end of transect CD. After 4.5 h of PGP (Fig. 4a), the $\overline{u}$ toward the southwest was observed at all transects.

Over a tidal cycle, the most noticeable change is the dramatic increase in current speed in transect BC during the DP. This strong flow (>1 m s^{-1}) is well known as the "jet-flow" derived from the reduction of the conveyance cross-section at a hydraulic structure (Cohen, 2012). Most of the study on the jet-flow at the TPP has been conducted through 2-D numerical modeling (Angeloudis et al., 2016; Xia et al., 2010), and the predicted flow patterns and the current speed were quite different from the observation results of this study. In the case of Swansea Bay Lagoon, similar to the topographical structure of the Sihwa TPP, the flow shape was a monotonous fan-shape with a maximum current speed of 0.9 m s^{-1} in $\overline{u}$. On the other hand, in this study, the location of the flow-enhancing region affected by the jet-flow was changed by the tidal variation, and the maximum current speed exceeded 1.4 m s^{-1} in $\overline{u}$. Furthermore, the asymmetry between the flood and ebb currents was often found due to the jet-flow (Valle-Levinson and Guo, 2009). Comparing the aforementioned velocity fields between DP and PGP, a significant asymmetry in current speed and direction was also observed in the vicinity of Sihwa TPP.

4.2. Comparison of velocity profiles between DP and PGP

The operation of the Sihwa TPP has an influence on the vertical velocity structures as well as horizontal flow patterns. To investigate

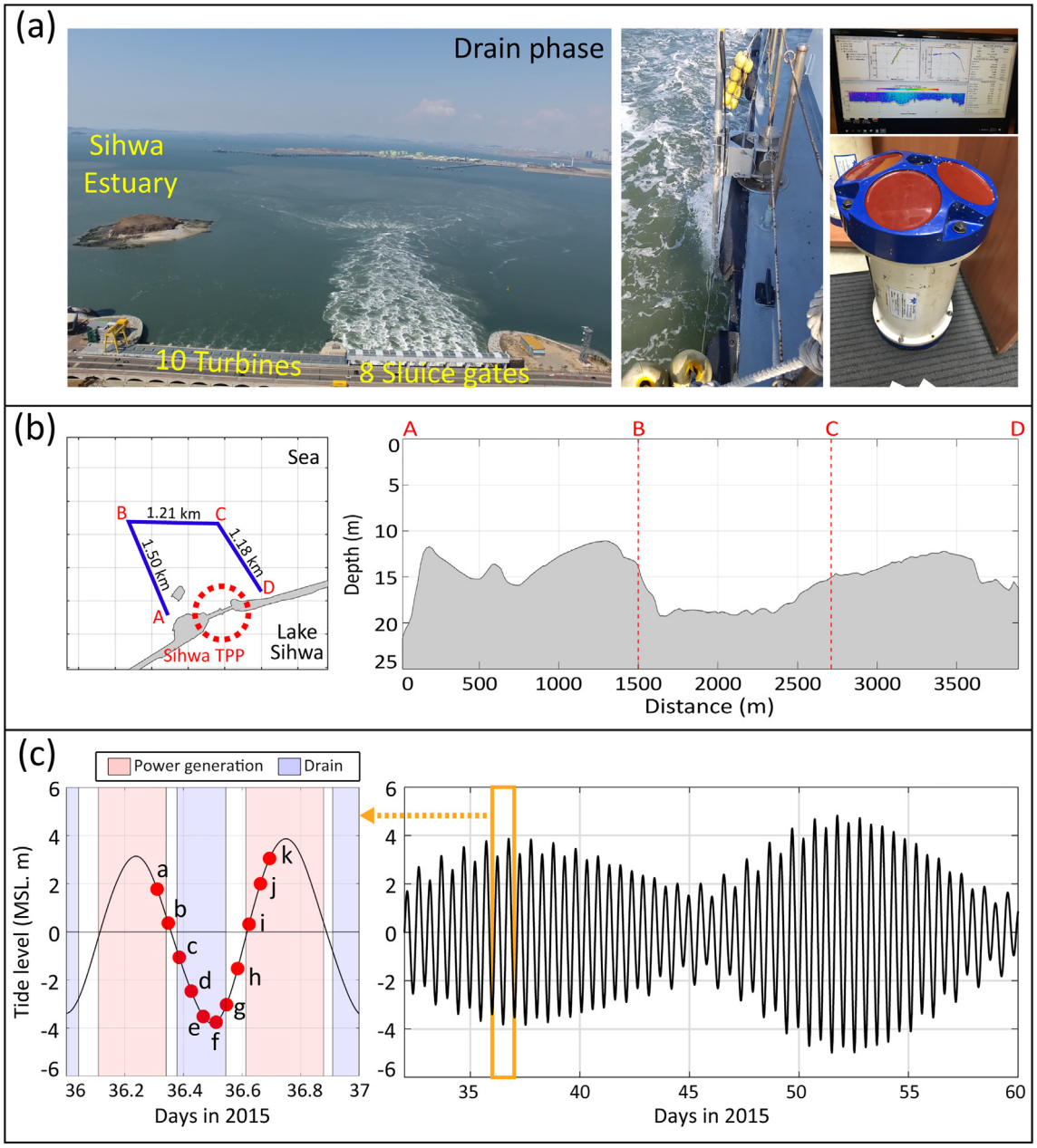


Fig. 2. (a) Photographs associated with the strong flow (>1.5 m s^{-1}) during the DP and real-time ADCP measurements along the transect lines, (b) the distance and depth variation along the ABCD, and (c) water level variations over the tidal cycles. The orange box in (c) indicates the observation period, and the detailed observation time is shown in the enlarged water level figure (represented by the red circles in (c)).

the variations in velocity profiles between PGP and DP, three time-windows for the early, middle, and end phases were selectively examined, as shown in Figs. 5 and 6.

Table 2
Summary of acoustic Doppler current profiler (ADCP) surveys conducted on February 5, 2015.

Transect	Observation time (hh:mm:ss)	Number of surveys	Mean survey duration (min)	Transect length (km)	Sampling rate (Hz)	Bin size (m)
AB	Start 07:03:55 End 16:18:53	11	19.27	1.50	2	0.5
BC	Start 07:20:04 End 16:47:56	11	13.18	1.21	2	0.5
CD	Start 07:00:10 End 16:31:06	11	14.68	1.18	2	0.5

In the early phases, the discharge effects on the velocity profiles in the entire water column were different. The current speed in the velocity profiles along ABCD early in the DP was weaker than that early in the PGP. During early DP (Fig. 5c), the current speed along the ABCD varied from 0.10 to 0.22 m s^{-1}, and the maximum surface-to-bottom current speed difference varied from 0.07 to 0.15 m s^{-1}. A stronger velocity difference occurred in transects BC and CD, compared to that in transect AB, which was adjacent to the small island with a weak current speed (<0.1 m s^{-1}) in the entire water column. In contrast, early in the PGP (Fig. 6i), the current speed along ABCD was up to two or more times stronger than that at early in the DP. On the other hand, the maximum surface-to-bottom current speed difference varied from 0.13 to 0.21 m s^{-1}, similar to the DP. In transect CD, the current speed was less than 0.20 m s^{-1} compared to that of the other two transects in both the DP and PGP periods.

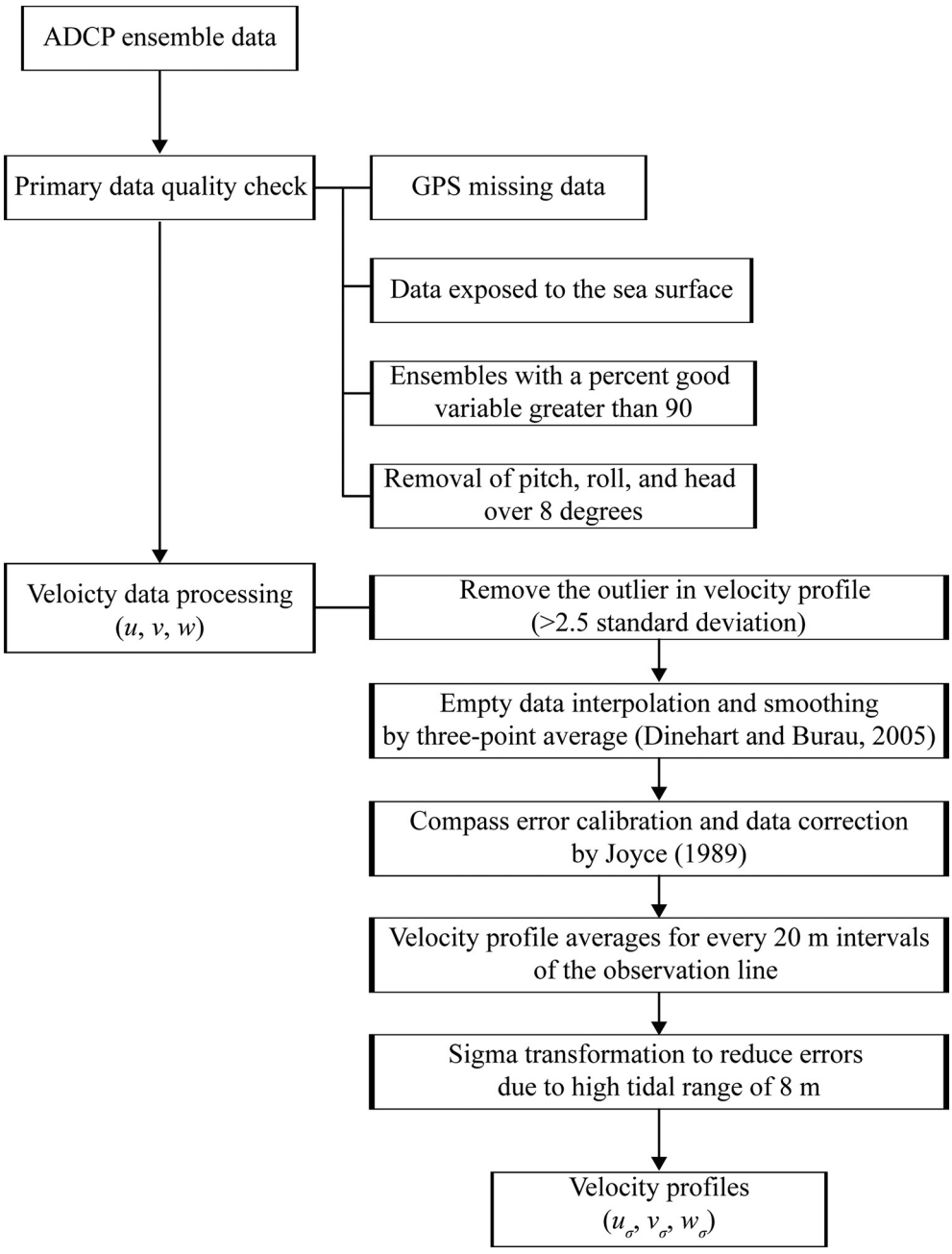


Fig. 3. Flowchart of extracting velocity profiles in sigma coordinate from ADCP ensemble data.

In the middle phases, the increase of speed in the velocity profiles occurred only in the DP, with a flow greater than 1.5 m s^{-1} occurring in the entire water column and not confined to the surface layer (Fig. 5e). The northwestward flow was mostly observed in transect BC, and the maximum current speed in the velocity profiles was about 2.27 m s^{-1}. During this period, a weak current speed (<0.25 m s^{-1}) was observed in both transects AB and CD. The maximum surface-to-bottom current speed difference varied from 0.05 to 0.41 m s^{-1}, showing a vertically homogeneous increase in the velocity profiles. At the middle of the PGP (Fig. 6k), the current speed was relatively weak compared to that of the early phase (Fig. 6i). The current speed at all transects was less than 0.35 m s^{-1}. The maximum surface-to-bottom current speed difference varied from 0.09 to 0.13 m s^{-1}.

In the end phases, the increase in the current speed during the DP was maintained, whereas that during the PGP was reduced. At the end of the DP, a strong current was still observed in transect BC with a width of about 250 m, but its position was changed to the eastern end of transect BC (Fig. 5g). The maximum current speed in velocity profiles was about 1.29 m s^{-1} along ABCD, and the maximum surface-to-bottom current speed difference varied from 0.10 to 0.18 m s^{-1}. Although the current speed in the BC decreased compared to that of the middle phase, it was more than twice as strong as the speed in other transects at the end phase. At the end of PGP, the current speed varied from 0.16 to 0.14 m s^{-1} in all transects (Fig. 6b). The maximum surface-to-bottom current speed difference varied from 0.07 to 0.10 m s^{-1}. These results suggested that the strength and direction of velocities in the vicinity of Sihwa TPP were mostly controlled by the discharge during DP and upstream discharge during PGP.

Overall, the jet-flow enhanced the horizontal velocity shear but has little effect on the increase of vertical velocity shear. Due to these shear characteristics, the jet-flow in downstream of Sihwa TPP may be closer to the convergence type than the divergence type. The jet-flow can be

Table 3
Operating data for drain and power generation phases (DP and PGP, respectively) on February 5, 2015. G1, G2 and G3 indicate the sluice gates of Sihwa tidal power plant (TPP) with and without the turbine, and sluice gate at the entrance of Lake Sihwa, respectively.

Phase	Sluice gates	Operating time (hh:mm)		Exchanged water volume ($\times 10^7$ m^3)
		Start	End	
Power generation	G1	02:38	08:11	8.75
		14:43	21:05	10.74
Drain	G1	00:00	00:50	0.29
		09:23	12:56	2.61
		22:10	24:00	1.46
	G2	00:00	01:00	1.11
		09:04	13:04	7.45
		21:50	24:00	4.51
	G3	00:00	01:00	0.14
		09:04	13:04	0.93
		21:50	24:00	0.56

classified into two types based on the vertical and horizontal flow structures (Broekema et al., 2018): divergence and convergence. In the divergence type, the jet-flow diverges widely in the horizontal plane. In order to preserve water volume, the return flow in opposite direction to the surface layer is found in the bottom layer due to vertical flow separation. In the convergence type, the entrained flow is found in both side channels of the main axis of the jet-flow and exits with a vertically consistent jet-flow throughout the water column. In terms of vertical flow structure observed at the Sihwa TPP, the one-way jet-flow in the entire water column was observed in a narrow area of transect BC during DP (Fig. 5e). In terms of horizontal flow structure (Fig. 5e and g), the flood current both the surface and bottom layer have begun at transect AB between the middle and end phases of the drain, while the reversed flow of flood current, is maintained at transect CD.

4.3. Instantaneous volume flux

To explain changes in the water volume transport due to tidal power generation, the temporal variability of Q at transects AB, BC, and CD is shown in Fig. 7. The positive and negative values in Q indicate the influx and outflux of water volume toward the ABCD region, respectively. The Q passing through transect AB exhibited the typical variations observed in estuary showing the standing wave characteristics, which water volume comes into the inside area of ABCD during the flood current and leaves during the ebb current. However, the magnitude between positive and negative Q through transect AB was unbalanced. The influx in transect AB during the rising tide reached about $+1.01 \times 10^4$ m^3 s^{-1}, whereas the outflux during falling tide decreased to about -0.49×10^4 m^3 s^{-1}.

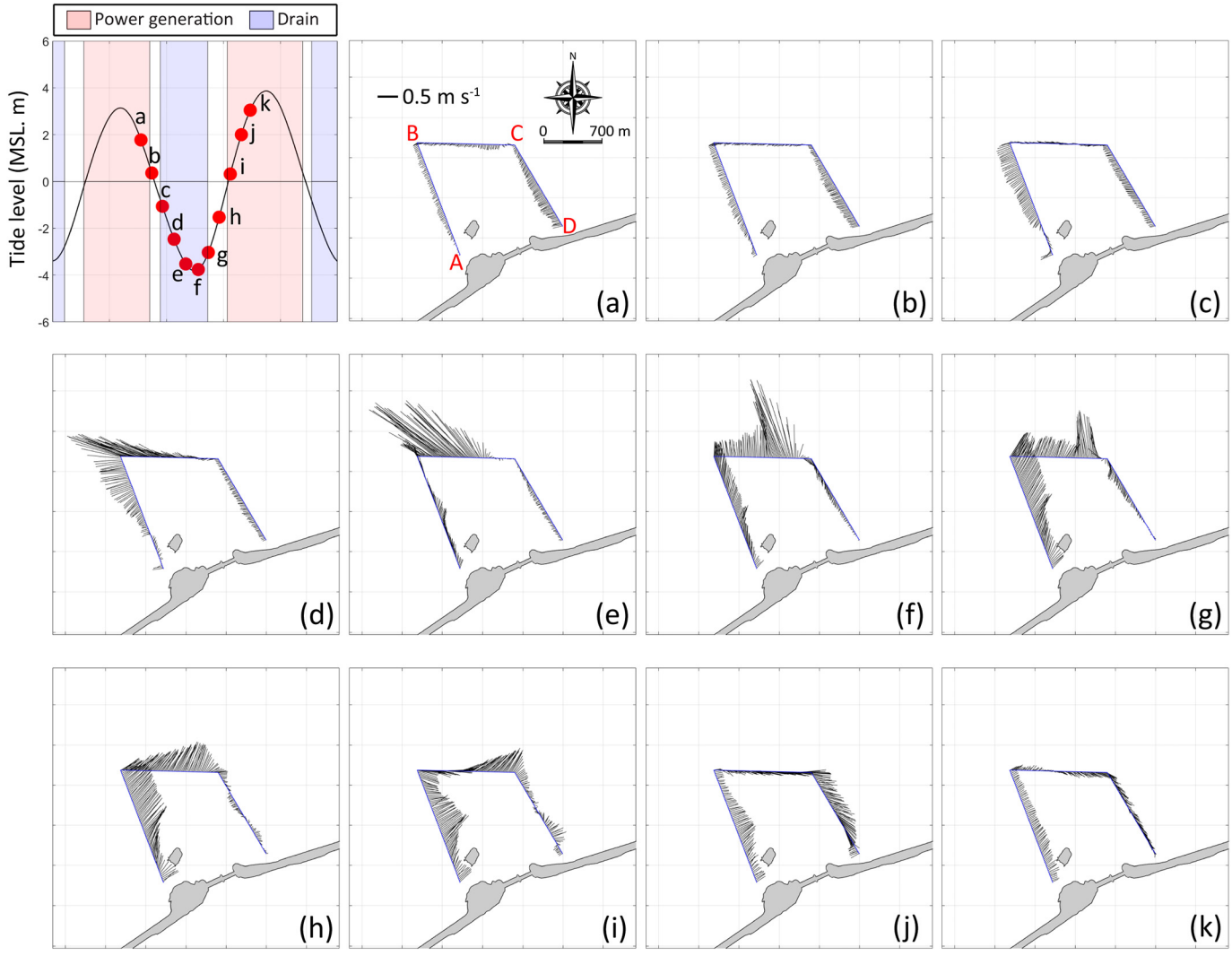


Fig. 4. Stick plots of the depth-averaged velocity over the entire observation period.

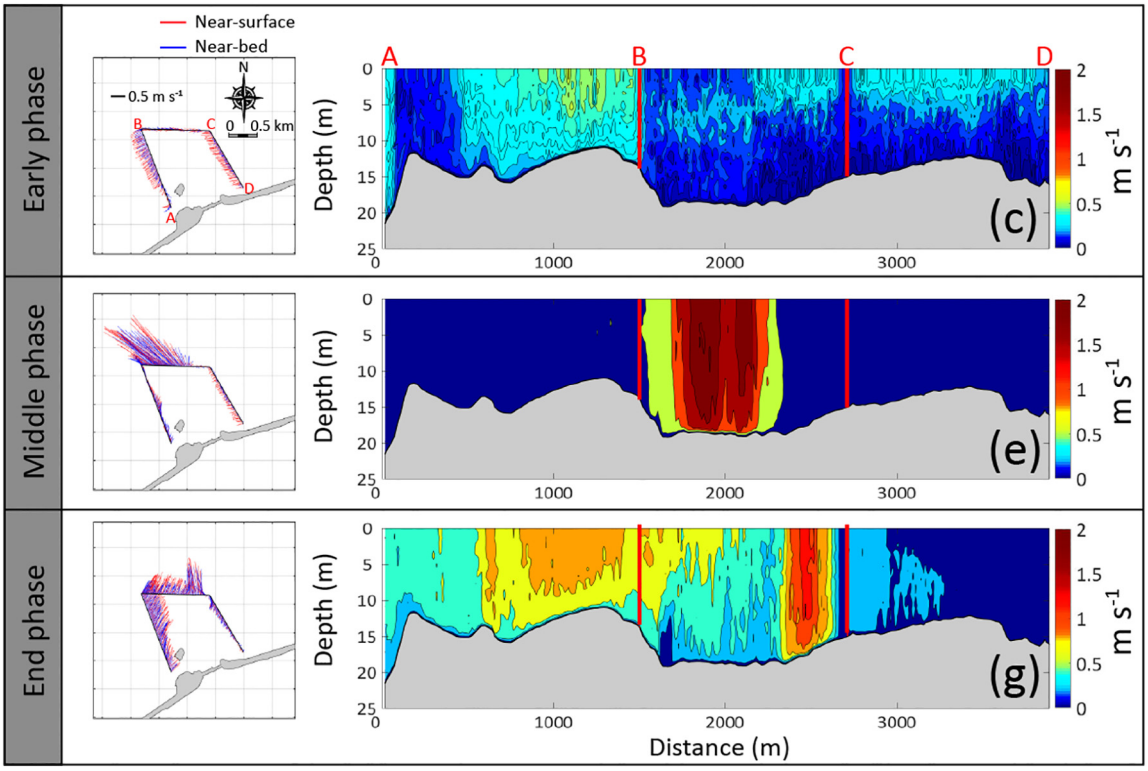


Fig. 5. Near-surface and -bed velocity fields, and current speed profiles along the ABCD during the DP: (c) early phase, (e) middle phase, and (g) end phase.

The Q in transect CD varied between -0.38×10^4 and $+0.49 \times 10^4$ m^3 s^{-1}, which was relatively lower than that in transect AB. During DP, the negative Q in transect AB turned positive, but the positive Q in transect CD remained constant for 3 h of the rising tide (e–g in Fig. 7b). Considering the short distance (<1.3 km), the Q toward the ABCD region in transect CD indicated that the water volume was

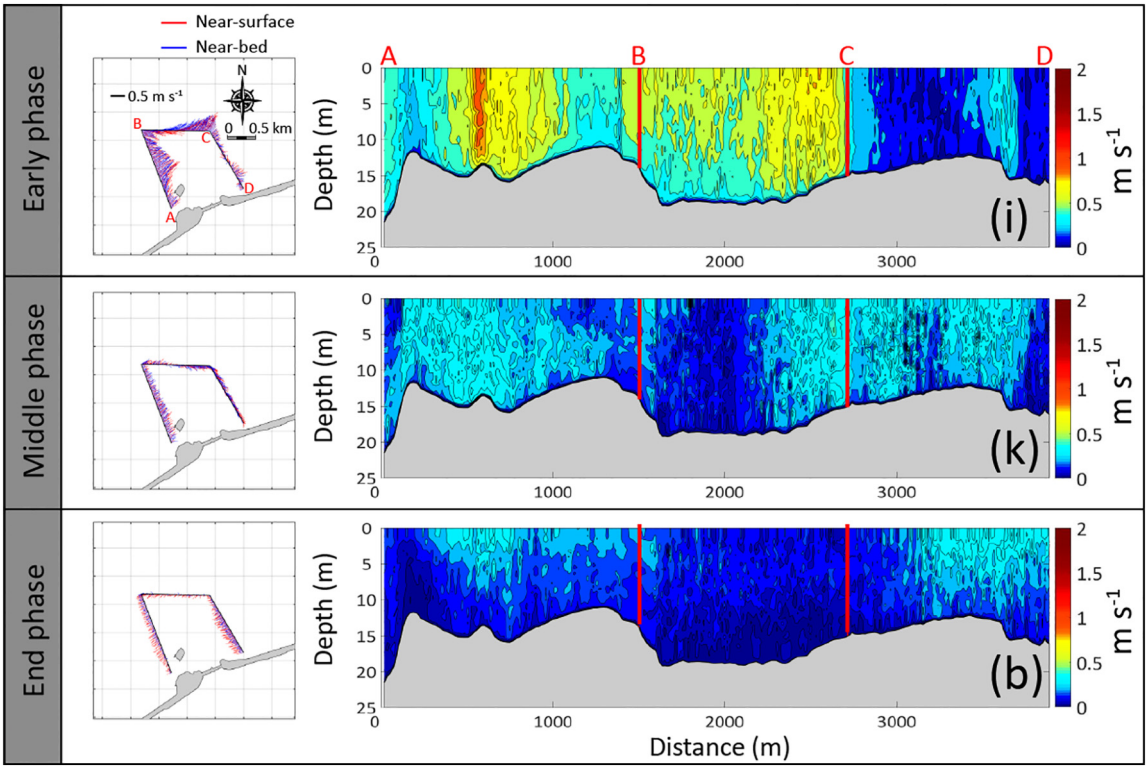


Fig. 6. Near-surface and -bed velocity fields, and current speed profiles along the ABCD during the PGP: (i) early phase, (k) middle phase, and (b) end phase.

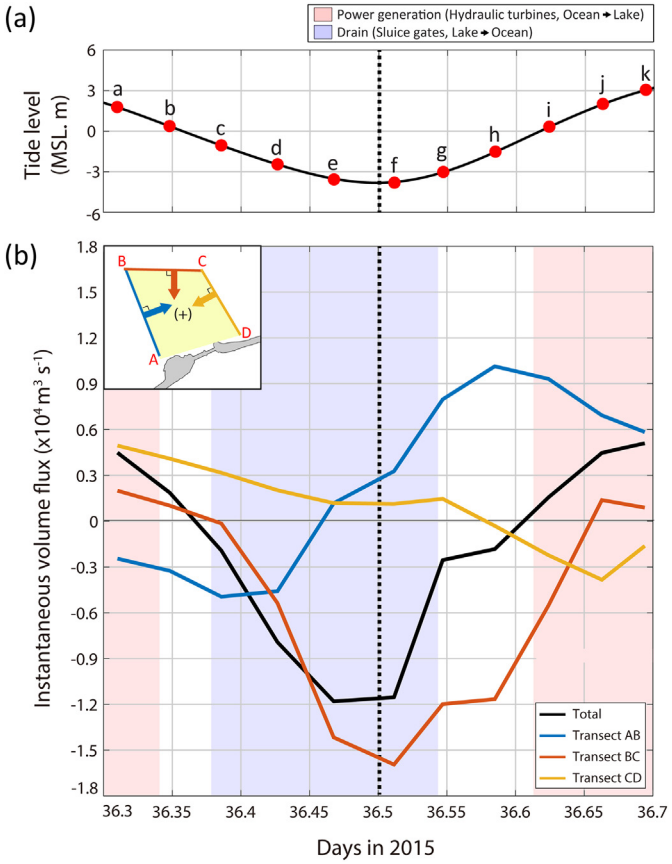


Fig. 7. Spatial and temporal variability of instantaneous volume fluxes in vicinity of Sihwa TPP: (a) water level, and (b) volume fluxes over a tidal cycle. In (a), the red circles indicate the time points at which observations were performed. In (b), the arrows in the upper left box represent the direction of the positive instantaneous volume flux of each transect. The black dotted lines mean low tide period.

temporarily entrained into the front of the Sihwa TPP due to the jet-flow. During these periods, the Q in transect BC was one order of magnitude higher than that in transects AB and CD, showing the maximum of 1.54×10^4 m^3 s^{-1}. This relatively high value was mostly attributed by the discharge rate of the Sihwa TPP, and eventually most of the water volume during DP was escaped through the transect BC.

5. Discussion

5.1. Effect of tidal power generation on the water mass exchange process

In the vicinity of artificial marine hydraulic structures such as surge barriers, sea dikes, tidal barrages, and dams in coastal regions, the impacts of jet-flow were well known (Vouriot et al., 2019). The highly sheared flow derived from the jet (>1.5 m s^{-1}) induced a bifurcation of the tidal current, resulting in the formation of a dipole vortex on both sides of the jet-flow (Bryant et al., 2012; Wells and van Heijst, 2003). This rotating flow can lead to the symmetrical entrainment process of ambient seawater (Geyer and Signell, 1990; Old and Vennell, 2001).

The characteristics of jet-flow and resultant water mass transport near the Sihwa area were slightly different from the balanced dipole vortex because of the characteristics of the discharge in a direction perpendicular to the tidal current (Fig. 8). The water mass transport was calculated by multiplying Q by the density of the seawater (ρ = 1023 kg m^{-3}). The directions for 0° and 90° in Fig. 8c indicate the northward and eastward transport, respectively. The most noticeable change associated with the operation of the Sihwa TPP was that the jet-flow was maintained in a narrow area of transect BC until the end of the DP (d–g in Fig. 8b). During these periods, the asymmetric entrainment processes of mass transport were observed on both sides of the jet-flow. The highest outflow of 574.6×10^3 kg s^{-1} for water mass transport toward the northwest corresponds to transect BC. During these periods, the highest mass transport in transects AB and CD were about 193.3 and 55.1 kg s^{-1}, respectively. As shown in the velocity fields (see Section 4.1), the flood current over transect AB started from the middle (Fig. 5e) toward the end (Fig. 5g) of the DP, while the reverse flow of the flood current was maintained at transect CD. Moreover, despite the longer duration of the flood current (e–k in Fig. 8) (e.g., ebb dominance), the maximum intensity of mass transport during flood current was greater than that during ebb current. This may have led to greater development of flood current at transect AB due to the attraction of jet flow. Thus, the water mass passing through transects AB and CD converges toward the jet-flow, but an asymmetric water mass transport may occur between transects AB and CD because of the discharge characteristics perpendicular to the background tidal current. If this asymmetry of mass transport was maintained for a long time, it could change the mixing of properties of tidal flow, as the water circulation leads to a barrier to transport across the perimeter (Provenzale, 1999).

In addition, asymmetry of mass transport during the operation of the Sihwa TPP can limit the source of materials entering and exiting upstream regions. To understand the detailed mass exchange processes affected by the operation of flood generation, the volume budget was estimated along the A′BCD′ transect lines. The A′A and DD′ were the unmeasured lines between the southern end of transects ABCD and the Sihwa tide embankment. The volume fluxes through the A′A and DD′ ($Q_{A'A}$ and $Q_{DD'}$) were estimated using the ratio extrapolation method suggested by Fulford and Sauer (1986) as follows:

$$Q_{A'A,DD'} = 0.3535 L d_m V_m \quad (2)$$

where V_m and d_m are the measured cross-sectional averaged velocity of the ADCP and the depth at the nearest position to the A′A and DD′, respectively. L is the distance between the Sihwa tide embankment and the last ADCP-measured position. The mean volume fluxes along the A′BCD′ transect lines are obtained by time-averaging Q values during the DP and PGP. The discharge rates of the DP and PGP are calculated using the total water volume and duration data suggested in Section 3. The discharge rate during the DP is about 6.99×10^3 m^3 s^{-1} corresponding to (c)–(g) periods. The discharge rate during PGP was derived from the average of 4.38×10^3 and 4.69×10^3 m^3 s^{-1}, corresponding to (a), (i), (j), and (k) periods. The positive and negative values of the volume flux indicate the fluxes entering and exiting the area surrounding A′BCD′, respectively.

On average, most of the water mass passing through the transects AB, CD, and gates of the Sihwa TPP during the DP escapes through the transect BC (Fig. 9a). There were one outflux and five influxes. During this period, the outflux only occurred in transect BC at about -9.52×10^3 m^3 s^{-1}. The major source of influx is the discharge of the DP and the influxes in transects AB and CD were relatively low at $+0.58 \times 10^3$ and $+1.80 \times 10^3$ m^3 s^{-1}, respectively. During this period, the $Q_{A'A}$ and $Q_{DD'}$ were both about $+0.05$ m^3 s^{-1}. The total influx ($+9.47 \times 10^3$ m^3 s^{-1}) was 0.05×10^3 m^3 s^{-1} lower than the total outflux (-9.52×10^3 m^3 s^{-1}). This suggests that the sediment accumulation in the sea route of the INP located in the northern part of the Sihwa TPP can be attributed to the sediment and materials through the upstream and transect CD. On the other hand, during the PGP (Fig. 9b), the influx of transect AB was about $+4.90 \times 10^3$ m^3 s^{-1}, which was at least 16 times greater than that at other lines. An outflux of -4.54×10^3 m^3 s^{-1}, which was more than 6 times the other outfluxes, occurred at the gates of the Sihwa TPP. Therefore, the major source of water mass entering the upstream was the transect AB. Interestingly, the influx patterns in transects A′A and DD′ were always estimated for both the DP and PGP. Among the complex mass exchange

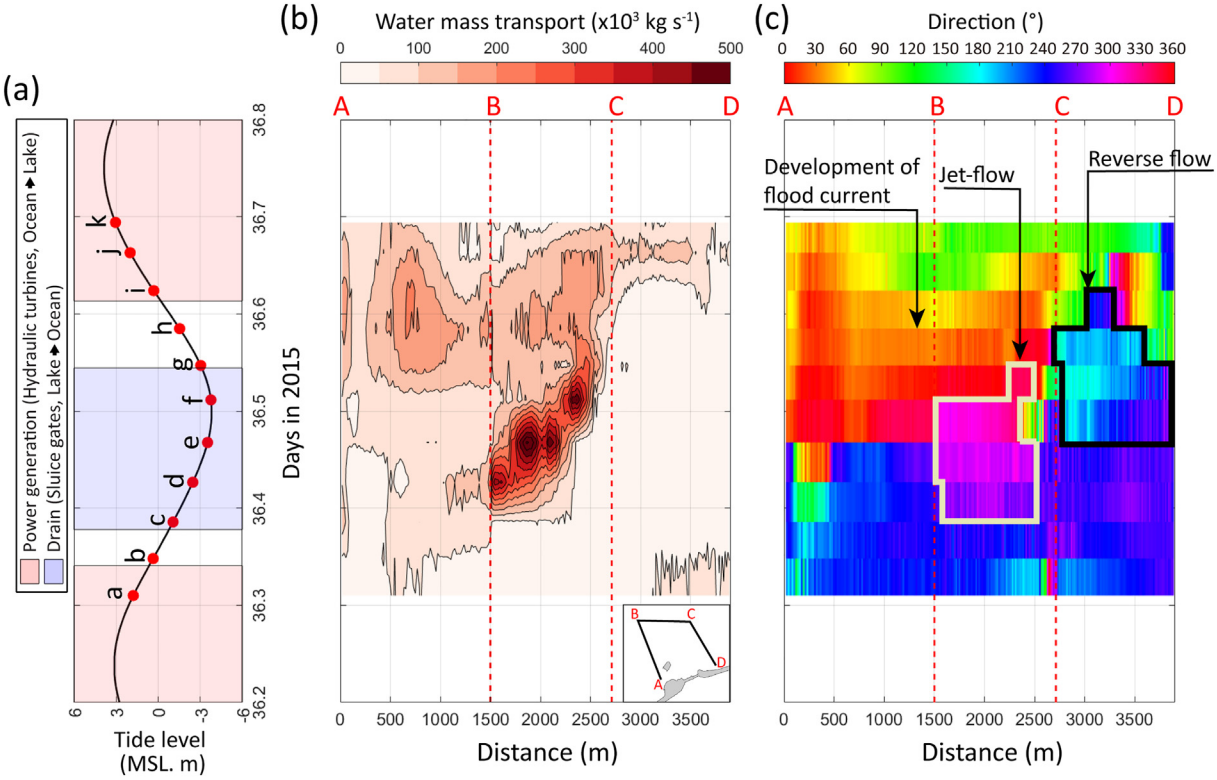


Fig. 8. The entrainment, transport and sorting of water mass by the jet-flow associated with jet-flow: (a) water level variations, (b) intensity, and (c) direction of water mass transport. In (c), the thick black and white lines indicate the reverse flow and jet-flow, respectively.

processes controlled by tidal power generation, consistent influxes in the region closest to the TPP can be the controlling factor in terms of migration of materials.

5.2. Implications

As discussed in this study, the environmental impact induced by tidal power generation can be both positive and negative. Changes in water mass exchange processes around TPPs have attracted attention worldwide, but mitigation measures remain almost entirely untested. Here, we carefully discuss practical issues related to the maritime safety and sedimentation of Lake Sihwa that need to be addressed urgently in the near future. We also expect that our suggestions will help to resolve practical issues in which tidal power is applied.

- The results of this study can be used to understand the risks on the main sea route downstream. In the northern part of the downstream of the Sihwa TPP, there are sea routes that accommodate large ship

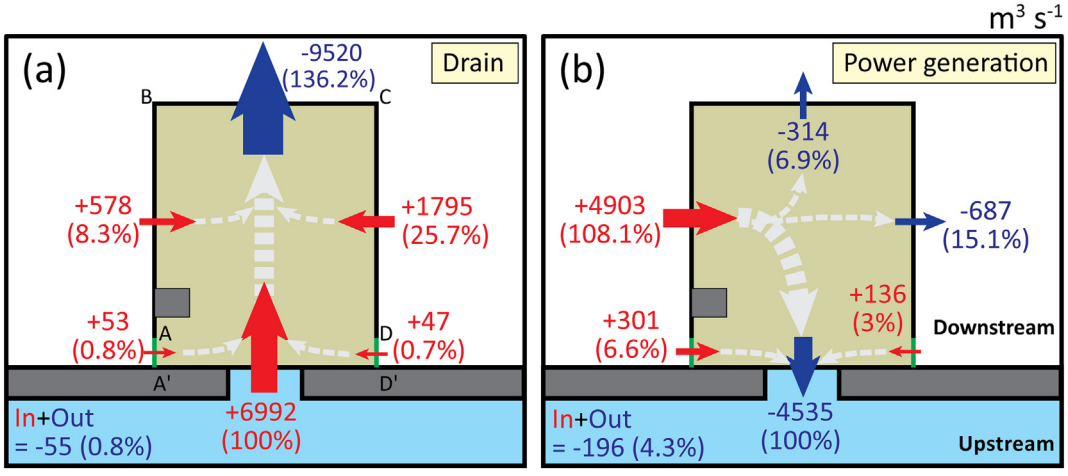


Fig. 9. Comparison of volume fluxes for each transect showing the difference of the water mass exchange between the (a) drain and (b) power generation phases. Note that the processes for the water mass exchange are simplified using the schematic diagrams. The black solid lines were three transect lines of ADCP, and the two green lines represent the edge lines, unmeasured regions. The volume fluxes at the unmeasured area ($Q_{A'A}$ and $Q_{DD'}$) were estimated using a ratio extrapolation method suggested by Fulford and Sauer (1986). The red and blue arrows indicate the rectangle box-in and -out fluxes, respectively. The size of blue and red arrows corresponds to the intensity of volume flux (values given in $m^3\ s^{-1}$). The percentages represent the contribution of box-in and -out flux. The thick and thin light gray dashed arrows show the main and minor flow patterns, respectively.

of LNG bases and Incheon New Port. Considering that the influence range of the jet-flow during the DP is about 2.5 km, the TPP can have a significant impact on the ship's operation. In addition, even after the DP is finished, the anticlockwise rotating vortex formed by the jet-flow has a secondary effect on the flow around the sea route. Because the duration of the operation of the Sihwa TPPs in the spring tide is more than 20 h per day, maritime safety issues associated with an increase in the current velocity are more vulnerable during spring tide than the period of neap tide. Therefore, it is necessary to secure the stability of the ship's operation by analyzing and predicting the influence range of the jet-flow according to the discharge intensity from the TPP during spring tide.

- The jet-flow concentrated in transect BC during DP presented in this study could be another risk factor for maritime safety associated with depth maintenance, along with the movement and sedimentation of suspended sediments. In an observational study by Kim et al. (2017), most of the suspended sediments during the DP moved toward the LNG base. In addition, the suspended sediments tend to move to the adjacent areas along the sea route with an anticlockwise rotating vortex. This means that sediments suspended in front of LNG bases are concentrated due to the jet-flow in a narrow area and are likely to settle, resulting in a decrease in the depth of the sea route. However, because it is limited to understanding the sediment movement of the whole sea route system using only the time series of SSC, observation and numerical modeling studies of sedimentation, resuspension, and settling of suspended sediments are necessary. In addition, since the concentration of sediments is affected by seasonal changes (e.g., freshwater discharge, or wind) as well as changes in flood-ebb and spring-neap variations, long-term data collection is necessary.
- The patterns of water mass exchange toward Lake Sihwa through transect AB during the PGP can be a source of sediment accumulation in Lake Sihwa. Since the operation of the Sihwa TPP began, there have been reports that the water depth of Lake Sihwa became shallower (Kim and Koo, 2015). Kim et al. (2021) suggested that most suspended sediments are steadily transported into the interior of Lake Sihwa and the fate of these sediments does not flow out during the DP but circulates in the dipole vortex. Therefore, downstream sediments can contribute to sediment accumulation in Lake Sihwa. However, since the observation data suggested in this study are limited to the downstream of the Sihwa TPP, there is a limitation in representing the entire system of Lake Sihwa as a characteristic of local sediment movement, so it is necessary to explain the detailed sediment transport through additional observations.

6. Conclusions

Tidal power generation is a research topic that is hardly monitored although they contribute to human activity and ensure stable electricity production. Hydrodynamic impacts of tidal power generation are a special issue for such a topic and require adequate monitoring and a full understanding of their hydrological functioning. In this study, the field measurements were conducted along the closed line in downstream of Sihwa TPP to investigate the effect of tidal power generation on the flow environment. For the first time, the spatiotemporal variations of flow patterns during power generation were presented through observational data. The results also showed that the tidal power generation induced asymmetry of water mass exchange between DP and PGP. The following conclusions are drawn from this study:

(1) The Sihwa estuary has undergone dramatic spatial flow pattern changes during tidal power generation. During the DP, jet-flow of 1.5 m s^{-1} or more was observed in a narrow area (<700 m) of transect BC. During this period, relatively weak current speeds were observed in transects AB and CD and their directions were opposite to each other. In contrast, the current speed during the PGP was weaker than that during DP, but it showed complex flow patterns, and a distinct reversed flow of flood current was formed near the TPP due to the entrainment flow.
(2) The jet-flow observed at transect BC induced a horizontally highly sheared flow along ABCD. However, the intensity and direction of the vertical velocity structures were quite homogeneous, and as a result, the vertical shear was quite weak. The disturbances of these velocity profile structures create barriers that inhibit water mass transport, resulting in an unbalanced intensity and direction of volume transport at AB and CD despite the same flood current phase.
(3) On average, asymmetry of the water mass transport entering and exiting upstream was clearly observed between DP and PGP. The water mass in the upstream during DP escapes through the transect BC with a volume flux of 9.52×10^3 m^3 s^{-1}, whereas that entering the upstream during PGP mostly flows through transect AB with a volume flux of 4.90×10^3 m^3 s^{-1}. Because these water mass exchange processes were repetitive and periodic cycles, they can contribute to the risk of maritime safety in the sea route of INP and sediment accumulation in Lake Sihwa in terms of long-term environmental changes.

The spatial observation data presented in this study include several limitations. The observed data for the current velocity along ABCD contain the effects of tide, the effects of discharge from a Sihwa TPP, and the combined effects of tide and discharge. It is difficult to decompose and analyze each effect using the observation currently being handled because there is a problem with the observation data length of 11 h. Also, since the discharge rate of TPP was determined by the water level difference between upstream and downstream, the spatiotemporal flow patterns between spring and neap tide may be different. However, considering the fact that the operation of TPP is mostly carried out during spring tide and the fact that there are few observational studies, the results of this study can be reviewed as comparative references and verification data for numerical modeling when the tidal power generation is planned in other regions in the future.

CRediT authorship contribution statement

J.W. Kim: Conceptualization, Methodology, Investigation, Software, Writing – original draft, Writing – review & editing, Visualization. **S.-B. Woo:** Supervision, Conceptualization, Methodology, Project administration, Writing – original draft, Writing – review & editing. **J.I. Song:** Methodology, Conceptualization, Writing – original draft, Writing – review & editing, Visualization. **H.-K. Kwon:** Project administration, Writing – review & editing, Resources.

Declaration of competing interest

The authors declare that they have no known competing financial interests or personal relationships that could have appeared to influence the work reported in this paper.

Acknowledgments

This research was supported by Basic Science Research Program through the National Research Foundation of Korea (NRF) funded by the Ministry of Education (NRF-2021R1I1A1A01060397). Also, this research was supported by a National Research Foundation of Korea Grant from the Korean Government (MSIT; the Ministry of Science and ICT) (NRF-2021M1A5A1075516) (KOPRI-PN21013).

References

Ahmadian, R., Falconer, R.A., Bockelmann-Evans, B., 2014. Comparison of hydro-environmental impacts for ebb-only and two-way generation for a Severn Barrage. Comput. Geosci. 71, 11–19. https://doi.org/10.1016/j.cageo.2014.05.006.

Angeloudis, A., Falconer, R.A., Bray, S., Ahmadian, R., 2016. Representation and operation of tidal energy impoundments in a coastal hydrodynamic model. Renew. Energy 99, 1103–1115. https://doi.org/10.1016/j.renene.2016.08.004.
Bae, Y.H., Kim, K.O., Choi, B.H., 2010. Lake Sihwa tidal power plant project. Ocean Eng. 37, 454–463. https://doi.org/10.1016/j.oceaneng.2010.01.015.
Bae, Y.H., Yoon, B.I., Seo, C.H., Park, S.J., Bang, K.-Y., Kwon, H.-K., Woo, S.-B., 2017. Residence time variation by operation of Sihwa tidal power plant in outer sea of Sihwa lake. J. Kor. Soc. Coast. Ocean Eng. 29 (5), 247–259. https://doi.org/10.9765/KSCOE.2017.29.5.247.
Broekema, Y.B., Labeur, R.J., Uijttewaal, W.S.J., 2018. Observations and analysis of the horizontal structure of a tidal jet at Deep Scour Holes. J. Geophys. Res.-Earth Surf. 123, 3162–3189. https://doi.org/10.1029/2018JF004754.
Bryant, D., Whilden, K., Socolofsky, S., Chang, K., 2012. Formation of tidal starting-jet vortices through idealized barotropic inlets with finite length. Environ. Fluid Mech. 12 (4), 301–319. https://doi.org/10.1007/s10652-012-9237-4.
Cham, D.D., Son, N.T., Minh, N.Q., Thanh, N.T., Dung, T.T., 2020. An analysis of shoreline changes using combined multitemporal remote sensing and digital evaluation model. Civ. Eng. J. 6 (1), 1–10. https://doi.org/10.28991/cej-2020-03091448.
Charlier, R.H., 2003. Sustainable co-generation from the tides: a review. Renew. Sustain. Energy Rev. 7, 187–213. https://doi.org/10.1016/S1364-0321(02)00011-4.
Cohen, C., 2012. Shallow-water Plane and Tidal Jets. Thesis, Doctor of philosophyUniversity of Otago. http://hdl.handle.net/10523/2493.
Dinehart, R.L., Burau, J.R., 2005. Averaged indicators of secondary flow in repeated acoustic Doppler current profiler crossings of bends. Water Resour. Res. 41, W09405. https://doi.org/10.1029/2005WR004050.
Fulford, J.M., Sauer, V.B., 1986. Selected papers in the hydrologic sciences. In: Subitsky, S.Y. (Ed.), Comparison of Velocity Interpolation Methods for Computing Open-channel Discharge, U.S. Geological Survey Water-Supply Paper 2290, pp. 139–144.
Geyer, W.R., Signell, R., 1990. Measurements of tidal flow around a headland with a shipboard acoustic Doppler current profiler. J. Geophys. Res.-Oceans 95, 3189–3197. https://doi.org/10.1029/JC095iC03p03189.
Giddings, S.N., Monismith, S.G., Fong, D.A., Stacey, M.T., 2014. Using depth-normalized coordinates to examine mass transport residual circulation in estuaries with large tidal amplitude relative to the mean depth. J. Phys. Oceanogr. 44, 128–148. https://doi.org/10.1175/JPO-D-12-0201.1.
Joyce, T.M., 1989. On in situ "Calibration" of shipboard ADCPs. J. Atmos. Ocean. Technol. 6, 169–172. https://doi.org/10.1175/1520-0426(1989)006<0169:OISOSA>2.0.CO;2.
Kadiri, M., Ahmadian, R., Bockelmann-Evans, B., Rauen, W., Falconer, R., 2012. A review of the potential water quality impacts of tidal renewable energy systems. Renew. Sustain. Energy Rev. 16 (1), 329–341. https://doi.org/10.1016/j.rser.2011.07.160.
Kang, Y.S., Chae, Y., Lee, H.R., 2013. Changes in sea water characteristics due to operation of Shihwa tidal power plant. J. Korean Soc. CoastOcean Eng. 25 (4), 219–235. https://doi.org/10.9765/KSCOE.2013.25.4.219.
Kim, M., Koo, B.J., 2015. The intertidal area in Lake Sihwa after operation of the tidal power plant. J. Korean Soc. Mar. Environ. Energy 18, 310–316. https://doi.org/10.7846/JKOSMEE.2015.18.4.310.
Kim, G., Lee, M.E., Lee, K.S., Park, J.-S., Jeong, W.M., Kang, S.K., Soh, J.-G., Kim, H., 2012. An overview of ocean renewable energy resources in Korea. Renew. Sustain. Energy Rev. 16, 2278–2288. https://doi.org/10.1016/j.rser.2012.01.040.
Kim, J.W., Ha, H.K., Woo, S.-B., 2017. Dynamics of sediment disturbance by periodic artificial discharges from the world's largest tidal power plant. Estuar. Coast. Shelf Sci. 190, 69–79. https://doi.org/10.1016/j.ecss.2017.03.029.
Kim, J.W., Ha, H.K., Woo, S.-B., Kim, M.-S., Kwon, H.-K., 2021. Unbalanced sediment transport by tidal power generation in Lake Sihwa. Renew. Energy 172, 1133–1144. https://doi.org/10.1016/j.renene.2021.03.088.
Kirby, R., Retière, C., 2009. Comparing environmental effects of Rance and Severn barrages. Proc. Inst. Civil. Eng.-Marit. Eng. 162, 11–26. https://doi.org/10.1680/maen.2009.162.1.11.
Lee, C.H., Lee, B.Y., Chang, W.K., Hong, S., Song, S.J., Park, J., Kwon, B.O., Khim, J.S., 2014. Environmental and ecological effects of Lake Shihwa reclamation project in South Korea: a review. Ocean Coast. Manag. 102, 545–558. https://doi.org/10.1016/j.ocecoaman.2013.12.018.
Mueller, D.S., Wagner, C.R., 2007. Correcting acoustic Doppler current profiler discharge measurements biased by sediment transport. J. Hydraul. Eng. 133, 1329–1336. https://doi.org/10.1061/(ASCE)0733-9429(2007)133:12(1329).
Nazarnia, H., Nazarnia, M., Sarmasti, H., Wills, W.O., 2020. A systematic review of civil and environmental infrastructures for coastal adaptation to sea level rise. Civ. Eng. J. 6 (7), 1375–1399. https://doi.org/10.28991/cej-2020-03091555.
O'Rourke, F., Boyle, F., Reynolds, A., 2010. Tidal energy update 2009. Appl. Energ. 87, 398–409. https://doi.org/10.1016/j.apenergy.2009.08.014.
Old, C.P., Vennell, R., 2001. Acoustic Doppler current profiler measurements of the velocity field of an ebb tidal jet. J. Geophys. Res. 106, 7037–7049. https://doi.org/10.1029/1999JC000144.
Park, Y.H., 2017. Analysis of characteristics of dynamic tidal power on the west coast of Korea. Renew. Sustain. Energy Rev. 68, 461–474. https://doi.org/10.1016/j.rser.2016.10.008.
Provenzale, 1999. Transport by coherent barotropic vortices. Annu. Rev. Fluid Mech. 31, 55–93. https://doi.org/10.1146/annurev.fluid.31.1.55.
Rtimi, R., Sottolichio, A., Tassi, P., 2021. Hydrodynamics of a hyper-tidal estuary influenced by the world's second largest tidal power station (Rance estuary, France). Estuar. Coast. Shelf Sci. 250, 107143. https://doi.org/10.1016/j.ecss.2020.107143.
Susaya, J., Kim, K.H., Chang, Y.-S., 2011. Characterization of major offensive odorants released from lake sediment. Atmos. Environ. 45, 1236–1241. https://doi.org/10.1016/j.atmosenv.2010.12.010.
Valle-Levinson, A., Atkinson, L.P., 1999. Spatial gradients in the flow over an estuarine channel. Estuaries 22, 179–193. https://doi.org/10.2307/1352975.
Valle-Levinson, A., Guo, X., 2009. Asymmetries in tidal flow over a Seto Inland Sea scour pit. J. Mar. Res. 67 (5), 619–635. https://doi.org/10.1357/002224009791218850.
Vouriot, C.V.M., Angeloudis, A., Kramer, S.C., Piggott, M.D., 2019. Fate of large-scale vortices in idealized tidal lagoons. Environ. Fluid Mech. 19, 329–348. https://doi.org/10.1007/s10652-018-9626-4.
Wells, M.G., van Heijst, G.F., 2003. A model of tidal flushing of an estuary by dipole formation. Dyn. Atmos. Oceans 37, 223–244. https://doi.org/10.1016/j.dynatmoce.2003.08.002.
Widén, J., Carpman, N., Castellucci, V., Lingfors, D., Olauson, J., Remouit, F., Bergkvist, M., Grabbe, M., Waters, R., 2015. Variability assessment and forecasting of renewables: a review for solar, wind, wave and tidal resources. Renew. Sustain. Energy. Rev. 44, 356–375. https://doi.org/10.1016/j.rser.2014.12.019.
Wolf, J., Walkington, I.A., Holt, J., Burrows, R., 2009. Environmental impacts of tidal power schemes. Proc. Inst. Civil. Eng.-Marit. Eng. 162, 165–177. https://doi.org/10.1680/maen.2009.162.4.165.
Wu, Y., Xu, C., Ke, Y., Chen, K., Xu, H., 2017. Multi-criteria decision-making on assessment of proposed tidal barrage schemes in terms of environmental impacts. Mar. Pollut. Bull. 125, 271–281. https://doi.org/10.1016/j.marpolbul.2017.08.030.
Xia, J., Falconer, R.A., Lin, B., 2010. Impact of different tidal renewable energy projects on the hydrodynamic processes in the Severn Estuary. Ocean Model 32, 86–104. https://doi.org/10.1016/j.ocemod.2009.11.002.
Yamini, O.A., Mousavi, S.H., Kavianpour, M.R., Ghaleh, R.S., 2021. Hydrodynamic performance and cavitation analysis in bottom outlets of dam using CFD modelling. https://doi.org/10.1155/2021/5529792 1-14.